ChemPubSoc Europe

DOI: 10.1002/open.201700192

Open Access ChemistryOPEN Full Papers

Macromolecular Crowding May Significantly Affect the Performance of an MRI Contrast Agent: A ^{1}H NMR Spectroscopy, Microimaging, and Fast-Field-Cycling NMR Relaxometry Study

Ren-Hao Cheng[+],[a] Jie-Min Chen[+],[a] Yu-Wen Chen,[b] Honghao Cai,[a, c, d] Xiaohong Cui,[c] Dennis W. Hwang,*[b] Zhong Chen,[c] and Shangwu Ding*[a]

Contrast enhancement agents are often employed in magnetic resonance imaging (MRI) for clinical diagnosis and biomedical research. However, the current theory on MRI contrast generation does not consider the ubiquitous presence of macromolecular crowders in biological systems, which poses the risk of inaccurate data interpretation and misdiagnosis. To address this issue, herein the macromolecular crowding effects on MRI contrast agent are investigated with the ^{1}H relaxation rate of water in aqueous solutions of Dotarem with different concentrations of macromolecules. Two representative macromolecular crowder systems are used: polyethylene glycol (with no specific secondary structure) and bovine serum albumin (with compact secondary and tertiary structures). The water ^{1}H relaxation rates in various solutions are measured in a fixed magnetic field and in variable magnetic fields. The results show significant crowding effects for both crowders. The relaxation rate is proportional to the concentration of the MRI contrast agent but shows conspicuous superlinearity with respect to the concentration of the crowder. The size of polyethylene glycol does not affect the relaxivity of water in Dotarem solutions. The above effects are verified with T_1- and T_2-weighted NMR microimages. These results highlight the importance of the effect of macromolecular crowding on the MRI contrast agent and are valuable for understanding the mechanism of MRI contrast agents and designing new-generation MRI contrast agents.

1. Introduction

Owing to its noninvasiveness, speed, and precision, magnetic resonance imaging (MRI)[1–3] has become one of the mostly used diagnostic methods for the detection of various kinds of diseases in hospitals[4–8] and for functional imaging in psychology and linguistics.[9,10] It has also been employed as a powerful tool for studying the structure, dynamics, and functions of numerous materials and systems in chemistry, materials science, physics, and biology.[2,11–13] A common theme among these subfields is the appropriate employment of MRI contrast agents to improve image contrast. Up to date, over 2000 MRI contrast agents (CAs) have been reported,[14–17] and many more are definitely to come.

It was recognized about 30 years ago that crowding and confinement effects are inevitable in a typical cellular environment in which thousands of different types of biomolecules coexist.[18–20] Intuitively, the crowding effect is a volume-excluding effect, because a part of the volume originally accessible to the studied molecules becomes unavailable with the presence of the crowding molecules, whereas confinement is the restriction on the motion of the studied molecules owing to the constraints of the environment. The two effects are clearly inter-

[a] R.-H. Cheng,[+] J.-M. Chen,[+] Dr. H. Cai, Prof. Dr. S. Ding
Department of Chemistry and Center for Nanoscience & Nanotechnology
National Sun Yat-sen University
70 Lien-Hai Road, Kaohsiung, Taiwan 80424 (Republic of China)
Fax: (886)-7-525-3909
E-mail: ding@mail.nsysu.edu.tw

[b] Dr. Y.-W. Chen, Dr. D. W. Hwang
Institute of Biomedical Sciences, Academia Sinica
Taipei (Taiwan) 115 (Republic of China)
E-mail: chedwh@ccu.edu.tw

[c] Dr. H. Cai, Dr. X. Cui, Prof. Dr. Z. Chen
Department of Electronic Science
Fujian Provincial Key Laboratory of Plasma and Magnetic Resonance
State Key Laboratory of Physical Chemistry of Solid Surfaces
Xiamen University
422 Siming South Road, Xiamen 361005 (P.R. China)

[d] Dr. H. Cai
School of Science, Jimei University
183 Yinjiang Road, Xiamen 361021 (P.R. China)

[+] These authors contributed equally to this work

Supporting Information and the ORCID identification number(s) for the author(s) of this article can be found under https://doi.org/10.1002/open.201700192.

twined, and it is sometimes difficult to differentiate them. Because of the importance of these effects, they have rigorously been investigated over the past three decades, and a large body of literature has appeared. The biophysical, biochemical, and physiological consequences of crowding and confinement, particularly in a cellular environment, such as protein folding and protein–protein interactions, have extensively been studied and published in hundreds of papers. Several comprehensive reviews on this topic are available.[21–30] However, many questions remain unanswered, and both experimental and theoretical investigations are still ongoing.[29,31]

With the development of in-cell nuclear magnetic resonance (NMR) spectroscopy,[32–39] the implication of these effects to the NMR spectroscopy of bio-macromolecules has been noticed in recent years. It has been shown, mostly through the work of the Pielak group,[40,41] for example, that macromolecular crowding may tremendously affect the translational and rotational diffusion of proteins and small molecules. Interestingly, the influence on translational diffusion and that on rotational diffusion may be very different. The consequence of macromolecular crowding on the dynamics of macromolecules and small molecules is currently under active investigation.

Because MRI contrast agents are in most cases administered into living things such as animals, human subjects, plants, tissues, and cells, the environment they surround is a typical crowded and confined space. Consequently, it seems straightforward to recognize that the relaxation enhancement of MRI contrast agents is influenced, probably by a significant magnitude, by crowding and confinement effects. To our best knowledge, however, there are only a few publications[42–48] reporting the systematic investigation of the possible effect of bio-macromolecules on MRI contrast and the crowding or confinement effects on the performance of MRI contrast agents. In our opinion, within the context of the relaxivity of the MRI contrast agent, crowding/confinement effects have at least two major consequences. The first is the excluded volume accessible to both small and large molecule-based contrast agents, with an excluded volume factor as large as 0.2.[29] This roughly converts into an increase in relaxivity by the same factor. This effect also exists for small molecules but is probably less significant because the relative excluded volume is much smaller for a small molecule (<0.01). The second consequence of crowding/confinement effects is that the number of water molecules (at which the observed spins are located) temporarily bound with the contrast agent is decreased, because it is entropically advantageous for large molecules to contact each other (so that small molecules have larger accessible spatial volume, which increases the entropy of the total system). We can infer that a contrast agent under real physiological conditions tends to have many large molecules surrounding it, which effectively reduces the accessibility to water (the imaged molecule).

Therefore, in this work, we report a systematic investigation on the effect of macromolecular crowding on the MRI contrast agent Dotarem (Figure 1). The representative crowding agents used in this work include polyethylene glycol (PEG) and bovine serum albumin (BSA) (Figure 1), both of which were used in previous work on studies of the crowding effect.[40,41] Both PEG and BSA are chosen because both are considered to have little or no specific interactions with other biomolecules so that the pure crowding effect can be exhibited. PEG has no definite secondary structure, whereas BSA has a highly fixed secondary structure, so the possible effect of the secondary structure can be revealed. The longitudinal relaxation rate in the bulk solutions is measured for each crowder at each concentration, which is then used as a reference to quantify the relaxivity enhancement of an MRI contrast agent in imaging experiments. Then, the spectra and images of specially designed phantoms (with water, contrast agent, and crowding agents in NMR tubes or capillaries) are acquired to obtain the relaxivity at various imaging settings. To supplement the experimental results, variable-field relaxation (NMR relaxation dispersion), which has been shown to be a useful tool for MRI contrast agents,[14–16,49] is also used to measure the longitudinal relaxation rate from 0 to 100 MHz. The results demonstrate that the macromolecular crowding effect may have a significant influence on the relaxivity of MRI contrast. The physical chemistry behind these results is analyzed, and the implications of the experimental findings on clinical MRI diagnosis and the development of new-generation MRI contrast agents are discussed.

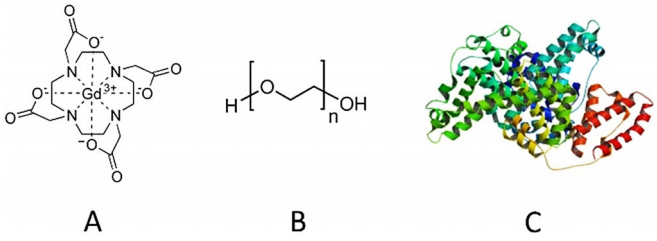

Figure 1. Molecules used in this work: a) MRI contrast agent Gd-DOTA (Dotarem), b) synthetic crowder polyethylene glycol (PEG), and c) protein crowder bovine serum albumin (BSA).

2. Results and Discussion

Figure 2 shows the ^{1}H longitudinal relaxation rate (R_1) of water in aqueous solutions of Dotarem and PEG. The concentration ranges for Dotarem and PEG were 0–40 mM and 0–40%, respectively. Five different PEG sizes, PEG200, PEG 2000, PEG6000, PEG10000, and PEG20000, were used. As can be seen from the three diagrams, the relaxation rate grows with the concentration of PEG but with a nonlinear (superlinear) trend. For example, at a Dotarem concentration of 30 mM, as the concentration of PEG changes from 5 to 10%, the relaxation rate increases from 200 to 215 s^{-1}, but if the concentration of PEG changes from 20 to 40%, the relaxation rate increases from to 285 to 485 s^{-1}. This is clear evidence that confirms that as the concentration of PEG increases, the intermolecular interaction between the PEG molecules becomes stronger so that there is an extra superposing effect on the rotational diffusion (hence relaxation rate). This is in agreement with previous observations of similar systems.[40,41] This nonlinear behavior cannot solely be attributed to volume-exclusion effects, because the excluded volume is proportional to the concentration of PEG. The excluded volume of PEG can be estimated on

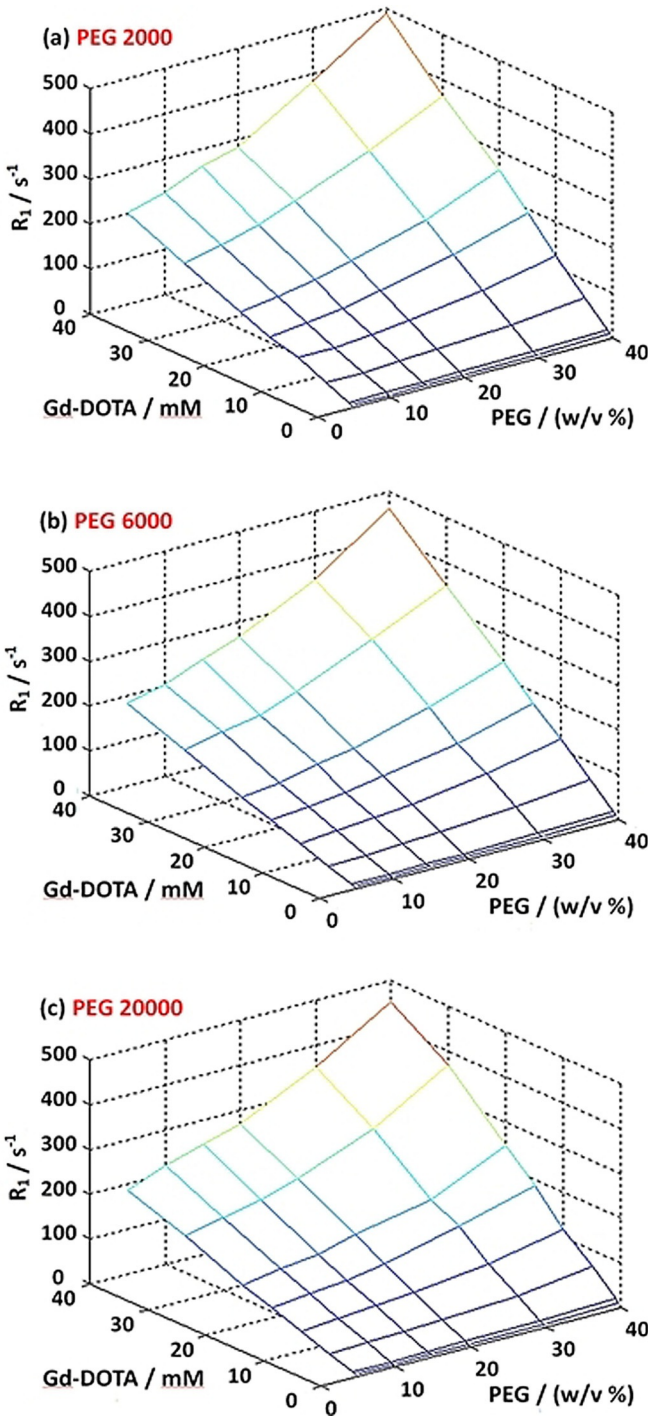

Figure 2. Longitudinal relaxation rate of water as a function of the concentrations of Dotarem (0, 5, 10, 20, 30, and 40 mM) and PEG crowder (5%, w/v; 10% w/v; 15%, w/w; 20%, w/v; 30%, w/v; 40%, w/v). PEG 200 (top), PEG 6000 (middle), and PEG 20000 (bottom).

the basis of the gyration radius of PEG (0.2 nm for PEG200) or the diameter (0.4 nm) and length of PEG (1.5 nm for PEG200). It is found that the exclusion of volume can only account for less than 20% of the increase in the relaxation rate for PEG200. This demonstrates that the macromolecular crowding effect has contributions other than a pure entropic effect if the concentration of the crowding macromolecules is high. It is well known that the viscosity of PEG increases with concentration.[40] Therefore, the relaxation rate increases with the concentration of PEG. If the concentration of PEG increases beyond a certain value, its viscosity increases superlinearly,[40] so the rotational diffusion correlation time of water also increases nonlinearly. This phenomenon shows that intermolecular interactions may have significant contributions to the macromolecular crowding effect. It is noteworthy that complete treatment of the relaxation rate in the presence of PEG needs to take into account the rotational diffusion of water molecules on PEG surfaces, and this leads to reorientation mediated by translational displacement (RMTD).[50,51] We do not perform this treatment in this work, but we do point out that this effect exists for other systems discussed in the rest of the paper.

As shown in Figure 2, the relaxation rate is proportional to the concentration of Dotarem. The absence of a nonlinear trend indicates that each water molecule is affected by only one molecule of the MRI contrast agent. This is simply because the concentrations were low (50 mM at most). If the concentration of Dotarem were to be increased to a value over 100 mM, a nonlinear relationship may be observed.[52] Because most medical diagnoses use low concentrations of MRI contrast agents, we did not use higher concentrations.

The interaction of PEG and the MRI contrast agent is also evidenced in Figure 2. At higher concentrations of Dotarem, the superlinearity of R_1 with respect to the concentration of PEG is increased, which indicates that the presence of Dotarem effectively amplifies the crowding effect of PEG on water relaxation. This implies that in MRI, if macromolecular crowders are present, the use of a contrast agent may further enhance the crowding effect.

A surprising phenomenon we observe from Figure 2 is that the relaxation rate is largely independent of the size of PEG, although it is slightly larger for larger sizes of PEG. The relaxation rates of the solutions with all three sizes of PEG show not only qualitative similarity but also quantitative equality. This implies that the influence of PEG on water diffusion is strictly localized. There is no long-range interaction between water and PEG. We attribute this behavior to the lack of secondary or higher order structures of PEG. For a polymer with only random loops, its size has no special effect on other molecules. Actually, the large size of a polymer molecule is equivalent to a higher concentration of a smaller sized polymer of the same kind. This size independence is interesting and is useful in the study of macromolecular crowding. We believe it is a common characteristic of structureless polymers. This prediction is confirmed with another polymer, sodium polyacrylate (NaPA), and its mixture with PEG, as given in the Supporting Information (Figure S1).

Figure 3 shows the change in the longitudinal relaxation rate of aqueous solutions of Dotarem as a function of the concentration of BSA and Gd^{3+} ions. Analogous to the cases for which PEG was used as a crowder, R_1 increases proportionally with the concentration of Gd^{3+}, probably because the highest concentration is only 40 mM. Moreover, the superlinearity of R_1 with respect to the concentration of the crowder and amplification of the crowding effect by Dotarem are also observed.

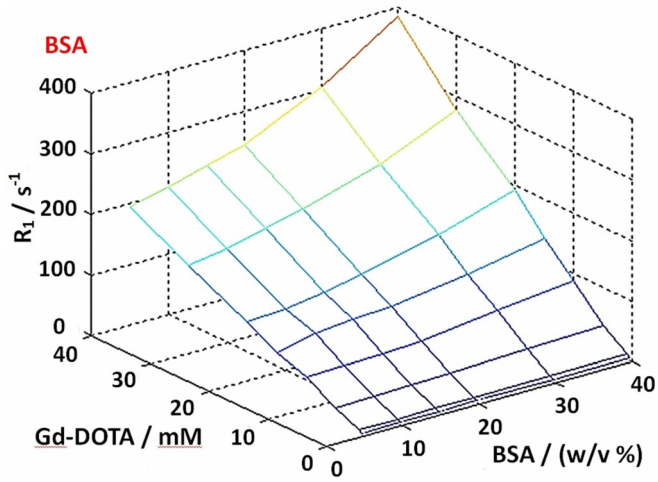

Figure 3. ^{1}H longitudinal relaxation rate of water as a function of the concentration of Dotarem (0, 5, 10, 20, 30, and 40 mM) and BSA (5, 10, 15, 20, 30, 40%, w/v).

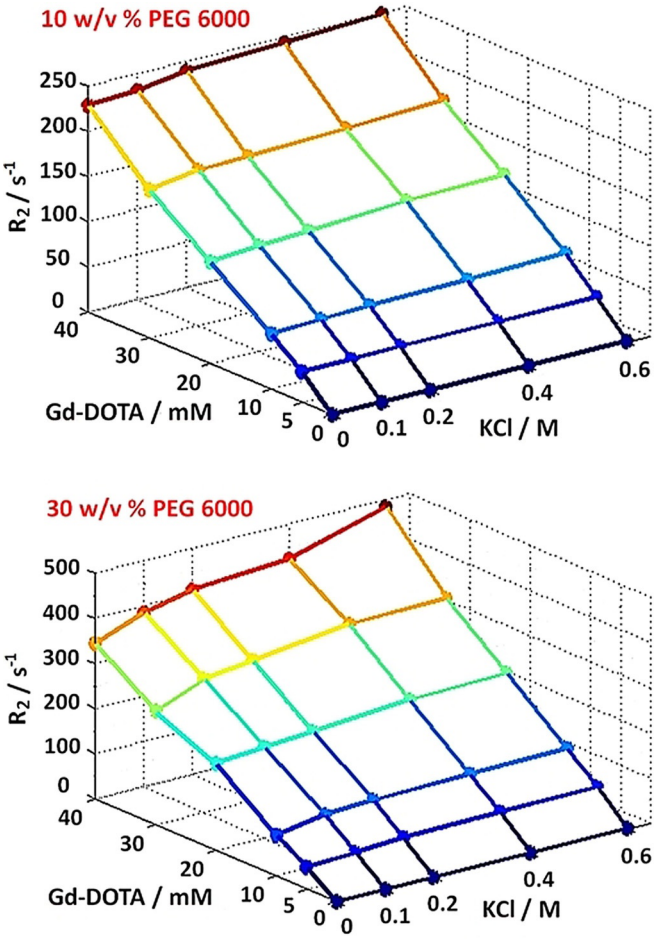

Figure 4. ^{1}H transverse relaxation rate of water as a function of the concentrations of Dotarem (0, 5, 10, 20, 30, and 40 mM), PEG6000 with 10% (w/v) (top), and 30% (w/v) (bottom) with concentrations of ions (K^+ and Cl^-; 0.0, 0.1, 0.2, 0.4, and 0.6 M).

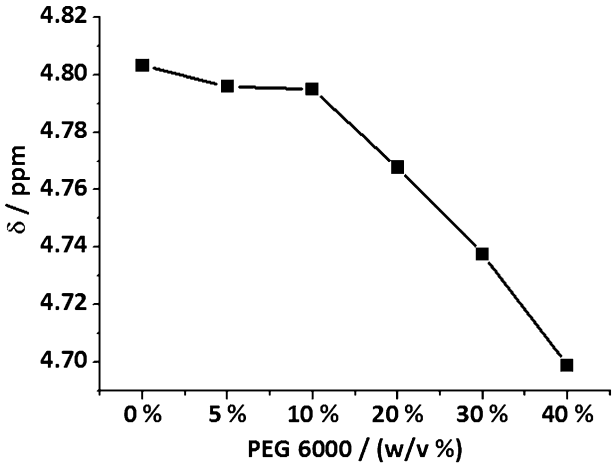

Figure 5. ^{1}H chemical shift of water as a function of the concentrations of PEG6000.

This shows the generality of the macromolecular crowding effect. However, the differences in the details are appreciable. For example, for all concentrations of Dotarem, R_1 of water in BSA solution is smaller than that in PEG solution of the same concentration. Consequently, the crowding effect of BSA is less significant than that of PEG. This can be explained by the fact that, in contrast to PEG, BSA has a compact secondary structure so that the interactions between BSA and water are statistically weaker than those between PEG and water. This phenomenon clearly demonstrates that the macromolecular crowding effect is not entirely volume exclusion and does depend on the specific structure of the crowder. As shown in Figure 4, the macromolecular crowding effect can also be observed for the transverse relaxation rate (R_2) of water. This is not unexpected, because both R_1 and R_2 are determined by the rotational diffusion of water. Consequently, in the MRI scan, if the T_1-weighted images are affected by the macromolecular crowding effect, then the T_2-weighted images may be equally affected. It is also found that the presence of ions in solution has a minor effect on R_2, although it increases with the concentration of PEG. Therefore, in the following, the effect of ions will not be further discussed.

In contrast to the pronounced changes in R_1 and R_2 by the macromolecular crowding effect, the change in the chemical shift of water is rather small, as shown in Figure 5. The ^{1}H chemical shift of water changes from a standard value of $\delta =$ 4.75 ppm to about $\delta = 4.52$ ppm at 40% of PEG. The decrease in the chemical shift can be understood by the fact that the hydrogen bonding between water and PEG is weaker than that between water molecules. The small change in the chemical shift as a result of the crowding effect is manifested by a smaller influence of the crowders on the structure than on the dynamics in a crowed system.[40]

Figure 6 shows the fast-field-cycling (FFC) relaxation dispersion curves of aqueous solutions of Dotarem (15 mM) with 5 and 40% (w/w) PEG6000 at two temperatures. It is found that the relaxation rate depends on the temperature, which can be explained straightforwardly because the rotational correlation time decreases at higher temperatures. The field dependence, however, is not trivial. At low PEG6000 concentrations such as

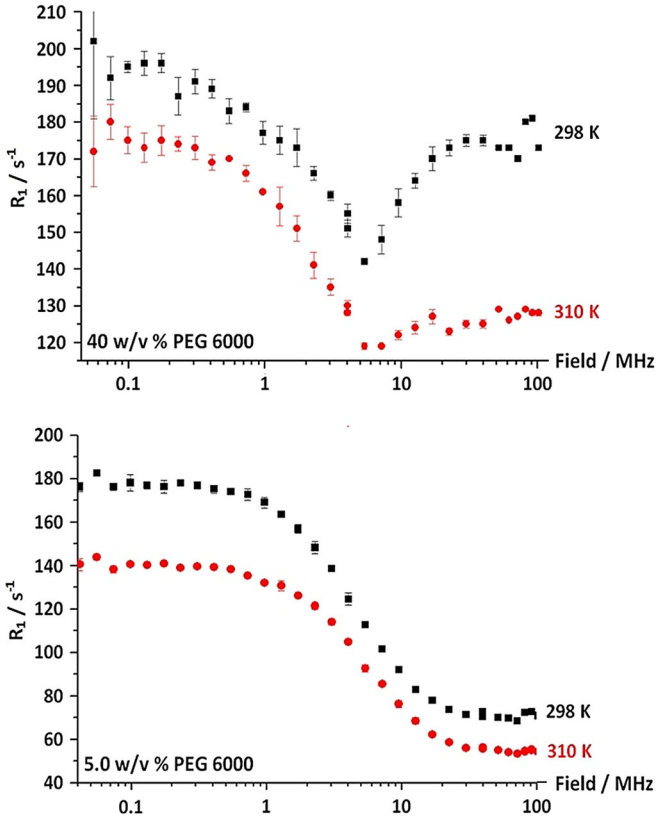

Figure 6. FFC ^{1}H relaxation dispersion curves of aqueous solutions of Dotarem (15 mM) with PEG6000 5% (w/w) (bottom) and 40% (w/w) (top) at two temperatures.

5% (w/w), the field dependence of the relaxation rate is monotonic, but at higher PEG6000 concentrations, it becomes non-monotonic. At lower fields (< 5.5 MHz), the relaxation rate decreases with the magnetic field, whereas at higher fields (> 5.5 MHz), the relaxation rate increases with the magnetic field. The turning point indicates that the critical correlation time of rotational diffusion can be found from the equations $\omega_m\tau_c \approx 1, \tau_c \approx 1.8 \times 10^{-7}$ s at 298 K and $\omega_m\tau_c \approx 1, \tau_c \approx 1.6 \times 10^{-7}$ (please define ω_m and τ_c) at 310 K, respectively; consequently, the correlation time increases with temperature, which is consistent with the previously reported results for water in materials[51] and biological systems.[53,54] The non-monotonic behavior of the water relaxation rate, which is commonly observed in nuclear magnetic relaxation dispersion (NMRD) profiles involving macromolecules and paramagnetic ions, is attributed to binding of the paramagnetic contrast agent molecules to the macromolecules (PEG6000 in our case).[55–58] Because of fast exchange between the water molecules on PEG and those on the of the MRI contrast agent, proton relaxation on PEG will affect water proton relaxation, which will lead to typical non-monotonic behavior.[55,57] Detailed analysis of this behavior is worthwhile but will not be discussed here, because it would be too tedious; nonetheless, it will be studied in the future.

The low-field trends are very similar for the two temperatures, but the high-field trends differ significantly. The FFC field-dependent relaxation rates at other Dotarem concentrations are given in Figure S2. The effect of crowding on the performance of the MRI contrast agent, therefore, is ubiquitous, regardless of the magnitude of the magnetic field in which the imaging scan is performed.

Figure 7 show the FFC relaxation dispersion curves of aqueous solutions of Dotarem (0, 0.5, 1, and 15 mM) with 5% (w/w) BSA at two temperatures. The turning point of the rotational correlation time was not observed within the magnetic field.

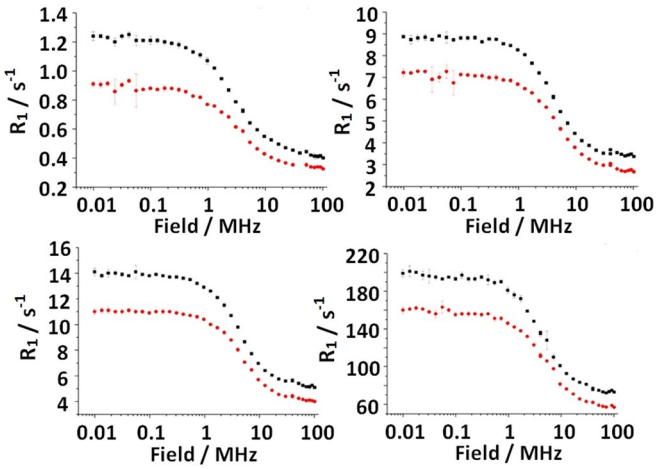

Figure 7. FFC ^{1}H relaxation dispersion curves of aqueous solutions of Dotarem (0, 0.5, 1, and 15 mM) with BSA 5% (w/v) at two temperatures.

Compared to the data shown in Figure 3 for BSA at 200 MHz, the turning point may be above 200 MHz. This phenomenon is worth mentioning, because we notice that BSA, with a molecular weight of 66 kDa, is much weightier than PEG6000. Its rotational correlation time should be longer than that of PEG. However, the concentration of BSA is only 5%, and its rotational diffusion correlation time is shorter than that of PEG with 40% (w/w). The small relaxation rate values also support this explanation.

To demonstrate directly the effect of crowding on MRI, a series of microimaging experiments were performed with a group of carefully designed image phantoms with different concentrations of the contrast agent and PEG crowder. Shown in Figures 8 and 9 are the T_1- and T_2-weighted images with different concentrations of Dotarem and different concentrations of PEG, respectively. For the T_2-weighted images, the high intensity corresponds to long T_2. In this work, the echo time (T_2 weighting) was 11 ms for all images to simplify analysis and highlight the effect of crowding on longitudinal relaxation. It is clear that the higher the concentration of Dotarem or PEG, the shorter the value of T_2, which leads to darker images. The crowding effect of PEG can be seen from a change in the intensity as the concentration of PEG increases. The nonlinear relationship can be seen from the intensity of each capillary with respect to the concentration of PEG. For T_1-weighted images, short recycle delays suppress the intensities of the images of the capillaries with longer T_1 values. If the recycle delay increases beyond a certain value, the intensities of all images are

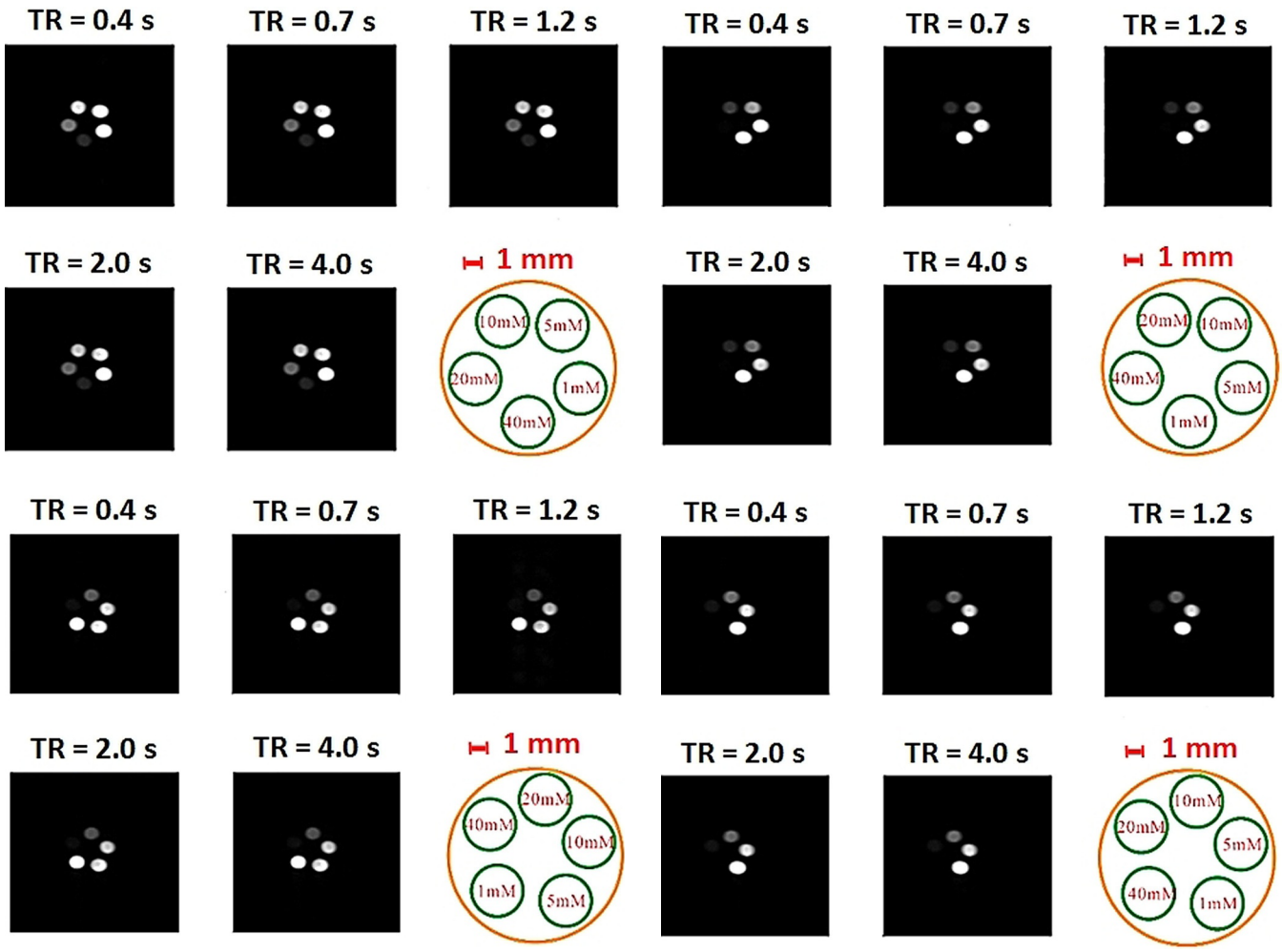

Figure 8. The T_1-weighted micro-MRI images of an aqueous solution of Dotarem with different concentrations of PEG: 5% (w/v) (top) and 20% (w/v) (bottom). In each image, the concentrations of Dotarem in the capillaries were 1, 5, 10, 20, and 40 mM, respectively, as indicated in the lower right side of each diagram. The recycle delays used for acquiring the images were 0.4, 0.7, 1.2, 2, and 4 s, respectively. The echo time (T_2 weighting) was 11 ms for all images.

Figure 9. The T_1-weighted micro-MRI images of aqueous solutions of Dotarem with different concentrations of PEG: 30% (w/v) (top) and 40% (w/v) (bottom). In each image, the concentrations of Dotarem in the capillaries were 1, 5, 10, 20, and 40 mM, respectively, as indicated in the lower right side of each diagram. The recycle delays used for acquiring the images were 0.4, 0.7, 1.2, 2, and 4 s, respectively. The echo time (T_2 weighting) was 11 ms for all images.

retained. The crowding effect of PEG on the images is seen by analyzing the intensities of the capillaries with respect to the concentration of PEG. Again, a nonlinear relationship is shown. Although these images were obtained with phantoms, the implication to imaging real materials such as biological systems is evident: the crowders in the imaged region will bring an additional weighting factor to both the T_1- and T_2-weighted images. Because Dotarem is primarily a T_1 contrast agent, the effect of crowding on the T_1-weighted images is also more significant. In light of these results and the ubiquitous presence of macromolecules in living organisms such as the human body, it is possible that in a real medical MRI image the crowding effect may bring extra complexity and even cause incorrect diagnosis. The consequence of the crowding effect on medical MRI will be presented in separate work.

Another consequence of the crowding effect on the MRI contrast agent is worth noting. With the extension of MRI applications to, in particular, in vivo biological systems and rapid imaging, the importance of large-sized MRI CAs was realized about two decades ago because they presumably provide high relaxivity in addition to the possibility of specificity (to tissue or protein). According to the prevalent theory of MRI contrast agents,[14–17] the rotational diffusion correlation time of the agent molecule, τ_R, is a controlling factor among other parameters such as the number of coordinated water molecules and the magnetic moment of the paramagnetic ion. Larger molecules have longer τ_R. Thus, a large number of MRI contrast agents based on polymers and supramolecules such as dendrimers have been reported over the past decade in the hope of obtaining higher relaxivity. However, it was found that the increased relaxivity resulting from an increase in the size of the molecule, although significant, was not as large as that expected from the perceived increase in τ_R based on current theory. This led to vigorous exploration of the understanding of this phenomenon.[15–17,59,60] It is suggested and widely accepted that these types of macromolecule-based MRI contrast agents,

having large sizes and long τ_R values for the entire molecule, also have high internal flexibility, which brings about a countereffect. By examining the analysis of previous publications, we found that this interpretation is at least incomplete. Our above results indicate that the crowding effect probably plays a significant role in reducing the relaxivity of polymer-based MRI contrast agents.

3. Conclusions

Using two representative crowder molecules, that is, polyethylene glycol (PEG) and bovine serum albumin (BSA), and a widely used magnetic resonance imaging (MRI) contrast agent, Dotarem, the effect of macromolecular crowding on a MRI contrast agent was studied for the first time with relaxation in constant and variable magnetic fields. The omission of the effect of macromolecular crowding in the current theory on MRI contrast agents has been proven to be unjustified. The major contributions from the macromolecular crowding effect were identified: 1) volume exclusion that increases effective concentration; 2) the structure and physicochemical properties of the crowder such as secondary and tertiary structures and hydrophilicity; 3) the reorientation mediated by translation displacement (RMTD) mechanism has an important contribution to relaxivity. The strong influence of macromolecular crowders on the performance of the MRI contrast agent suggests the necessity of taking into account the macromolecular crowding effect in medical diagnosis, animal/plant imaging, cellular imaging or imaging gene expression, molecular recognition or other chemical or biochemical events, as well as in the development of new-generation MRI contrast agents.

Experimental Section

Sample Description and Preparation

The commercial MRI contrast agent Dotarem (each bottle with 20 mL, 0.5 M), purchased from Guerbet Co., Ltd, Taiwan, was used in this work, the molecular structure of which is shown in Figure 1a. It was used as purchased without further purification. Dotarem is the most employed MRI contrast agent in medical diagnosis and is also the benchmark for NMR relaxivity measurements. Dotarem (5, 10, 50, 100, 150, 200, 300, and 400 μL) was added into a flask, and then the appropriate amount of pure water (deionized with a resistivity larger than 0.5 MΩ cm) was added to prepare different solutions (0.5, 1, 5, 10, 15, 20, 30, and 40 mM). Polyethylene glycol (PEG, Figure 1b) with five molecular weights (200, 2000, 6000, 10000, and 20000) was purchased from Sigma–Aldrich (purity > 99%). The five PEG samples are named PEG200, PEG2000, PEG6000, PEG10000, and PEG20000. Six concentrations for each type of PEG were used: 5, 10, 15, 20, 30, and 40% (w/v, g mL^{-1}). The samples were prepared by adding 0.25, 0.5, 0.75, 1, 1.5, and 2 g of PEG and 15% D_2O (w/w) into a 5 mL flask with a sonicator to assist dissolution of PEG.

Bovine serum albumin[61] (BSA, Figure 1c) was purchased from Union Biomed, Inc. (Taiwan) with a purity > 99%. Six concentrations, 5, 10, 15, 20, 30, and 40% (g mL^{-1}), were prepared by following three steps. First, 10× phosphate buffer solution (10×PBS) was prepared. NaCl (40 g), Na_2HPO_4 (7.2 g), KH_2PO_4 (1.2 g), and KCl (1 g) were added into a flask, and then water was added until the total volume reached 500 mL. Second, 1× phosphate buffer solution (1×PBS) was prepared. 10×PBS (2 mL) was taken into a flask, and 15% D_2O was added until the total volume reached 20 mL. Dilute HCl and NaOH solutions were added as need to adjust the pH to 7.4. Third, the BSA solution was prepared. BSA (0.25 g) was added to a flask, which was followed by the addition of 1×PBS (400 μL), and the mixture was sonicated at 40 °C to dissolve BSA. Then, 1× PBS was added until the total volume reached 5 mL to prepare a 5% (*g*/*g*) BSA solution. Other concentrations (10, 15, 20, 30, and 40%) could be made by adding more BSA into the solution. If bubbles appeared, the sample was placed into a fridge at 4 °C for a few days until all bubbles disappeared.

NMR Spectrum and Relaxation Measurements

Spectrometer: All NMR spectroscopy experiments were performed with a Varian Mercury liquid-state 200 NMR spectrometer operating at 4.7 T (resonance frequency of 200 MHz for protons) at room temperature (25 °C).

Pulse sequence: The pulse sequences used included single-pulse and inversion-recovery pulse sequences for recording NMR spectra and relaxation rate measurements. Chemical shifts were referenced to tetramethylsilane, which was filled in a specially designed capillary inside the NMR tube.

Pulse parameters: The 90° pulse was 13.5 μs with an RF power of 18.5 kHz (25 dB). The repetition delays were set according to the estimated T_1 values. For high concentrations of Dotarem, T_1 could be very short so the delay could be set to a small value to save experimental time. The delays between the 90° pulse and the 180° pulse were also decided by the estimated T_1 values to ensure a full relaxation–recovery curve.

NMR Microimaging

Phantom preparation: Each sample of a given concentration of Dotarem and crowder was sealed in a capillary (0.8–1.1×90 mm) with wax to prevent sample vaporization. Each capillary was marked with a specific color to label the concentration. All six capillaries were then placed into a polystyrene tube (outer diameter: 4 mm, length 2 cm) and sealed with wax to prevent relative motion of the capillaries during imaging experiments.

Imaging parameters: All NMR microimaging experiments were performed with a Varian Innova solid-state 500 NMR spectrometer operating at 11.7 T (resonance frequency of 500 MHz for protons) at room temperature (25 °C). The detected nuclear spins were water protons. The pulse sequence used was spin echo multiple slice (SEMS) with a sinc-shaped excitation pulse (90°) of 2 ms and power of 22 dB, a sinc-shaped refocusing pulse (180°) of 2 ms and power 28 dB. The slice selection gradient field was 5.21732 G c^{-}. The phase-encoding gradient fields were switched between −10.0 and 10.0 G c^{-} with a step size of 0.156 G c^{-}, and the frequency-encoding gradient field was 12.862 G c^{-}. The field of view was 1 cm× 1 cm. A total of 128 steps were used for phase encoding, and 256 points were acquired in the frequency-encoding dimension. The spin echo times (TE) used were between 10 and 120 ms (typically seven values were selected). Total single scan times (TR) were between 0.06 and 4 s, depending on the relaxation recycle delay used.

NMR Relaxation Dispersion

Measurements of the field-dependent relaxation rate were performed by using a fast-field-cycling (FFC) NMR relaxometer (SMARtracer, Stelar S.r.l, Italy). The field ranged from 2.35×10^{-4} to 2.35 T (corresponding to a proton Larmor frequency range of 0.01 to 100 MHz). The pulse sequence used was the classical saturation–recovery sequence. The acquisition field was 16 MHz, and the dead time of the spectrometer was about 10 μs. The temperature was controlled with a VTC90 temperature controller over the temperature range of 298 and 310 K with a precision of 0.1 K.

Data Analysis

Relaxation rates were obtained by fitting the recovery curve (with exponential growth) with the built-in software on the spectrometer. The relationships between relaxation rate and concentration of the MRI contrast agent and the concentration of the macromolecular crowder were drawn with the data analysis software RHC012.

Acknowledgements

This work was supported by the Ministry of Science and Technology of the Republic of China (Nos. MOST 103–2113-M-110 -006 and MOST 104–2113-M-110-010 to S.D. and MOST 103–2113-M-194-005 to D.W.H.), the National Natural Science Foundation of China (Grant Nos. 21327001 and 11375147 to Z.C.), the National Natural Science Foundation of Fujian Province (Grant No. 2016J01078 and 2017J05011 to H.C.), and the Fundamental Research Funds for the Central Universities (Grant No. 20720160125 to X.C.).

Conflict of Interest

The authors declare no conflict of interest.

Keywords: imaging agents · macromolecular crowding effect · magnetic resonance imaging · NMR spectroscopy · relaxivity

[1] Z. P. Liang, P. C. Lauterbur, *Principles of Magnetic Resonance Imaging: A Signal Processing Perspective*, Institute of Electrical and Electronics Engineers, New York, **2000**.
[2] M. T. Vlaardingerbroek, J. A. Boer, *Magnetic Resonance Imaging: Theory and Practice*, Springer Science & Business Media, Berlin, **2013**.
[3] M. A. Bernstein, K. F. King, X. J. Zhou, *Handbook of MRI Pulse Sequences*, Elsevier, Amsterdam, **2004**.
[4] F. A. Burgener, S. P. Meyers, *Differential Diagnosis in Magnetic Resonance Imaging*, Thieme, Stuttgart, **2011**.
[5] D. W. Stoller, *Magnetic Resonance Imaging in Orthopaedics and Sports Medicine, Vol. 1*, Lippincott Williams & Wilkins, Baltimore, MD, **2007**.
[6] S. W. Atlas, *Magnetic Resonance Imaging of the Brain and Spine Vol. 1*, Lippincott Williams & Wilkins, Philadelphia, PA, **2009**.
[7] D. Le Bihan, R. Turner, P. Douek, N. Patronas, *AJR Am. J. Roentgenol.* **1992**, *159*, 591 – 599.
[8] D. A. Sipkins, D. A. Cheresh, M. R. Kazemi, L. M. Bednarski, *Nat. Med.* **1998**, *4*, 623 – 626.
[9] R. B. Buxton, *Introduction to Functional Magnetic Resonance Imaging: Principles and Techniques*, Cambridge University Press, Cambridge, **2009**.
[10] K. A. Stigler, B. C. McDonald, A. Anand, A. J. Saykin, C. J. McDougle, *Brain Res.* **2011**, *1380*, 146 – 161.
[11] B. Blumich, *Monographs on the Physics and Chemistry of Materials Vol. 57: NMR Imaging of Materials*, Oxford University Press, Oxford, **2000**.
[12] I. A. Farhat, P. S. Belton, G. A. Webb, *Magnetic Resonance in Food Science: From Molecules to Man*, Royal Society of Chemistry, Cambridge, **2007**.
[13] K. J. Bradford, H. Nonogaki, *Seed Development, Dormancy and Germination*, Blackwell, Oxford, **2007**.
[14] R. B. Lauffer, *Chem. Rev.* **1987**, *87*, 901 – 927.
[15] P. Caravan, J. J. Ellison, T. J. McMurry, R. B. Lauffer, *Chem. Rev.* **1999**, *99*, 2293 – 2352.
[16] *The Chemistry of Contrast Agents in Medical Magnetic Resonance Imaging* (Eds.: A. E. Merbach, É. Tóth), Wiley, Chichester, **2001**, Vol. 46.
[17] A. Accardo, D. Tesauro, L. Aloj, C. Pedone, G. Morelli, *Coord. Chem. Rev.* **2009**, *253*, 2193 – 2213.
[18] A. Minton, J. Wilf, *Biochemistry* **1981**, *20*, 4821 – 4826.
[19] A. B. Fulton *Cell* **1982**, *30*, 345 – 347.
[20] A. P. Minton, *Mol. Cell. Biochem.* **1983**, *55*, 119 – 140.
[21] D. Hall, A. P. Minton, *Biochim. Biophys. Acta. Proteins Proteomics.* **2003**, *1649*, 127 – 139.
[22] G. Rivas, F. Ferrone, J. Herzfeld, *EMBO Rep.* **2004**, *5*, 23 – 27.
[23] H. X. Zhou, *Acc. Chem. Res.* **2004**, *37*, 123 – 130.
[24] H. X. Zhou, *Biochemistry* **2004**, *43*, 2141 – 2154.
[25] A. P. Minton, *J. Pharm. Sci.* **2005**, *94*, 1668 – 1675.
[26] A. P. Minton, *J. Cell Sci.* **2006**, *119*, 2863 – 2869.
[27] R. J. Ellis, A. P. Minton, *Biol. Chem.* **2006**, *387*, 485 – 497.
[28] H. X. Zhou, *Arch. Biochem. Biophys.* **2008**, *469*, 76 – 82.
[29] H. X. Zhou, G. Rivas, A. P. Minton, *Annu. Rev. Biophys.* **2008**, *37*, 375.
[30] J. A. Dix, A. Verkman, *Annu. Rev. Biophys.* **2008**, *37*, 247 – 263.
[31] T. Ando, J. Skolnick, *Pro. Natl. Acad. Sci.* **2010**, *107*, 18457 – 18462.
[32] Z. Serber, A. T. Keatinge-Clay, R. Ledwidge, A. E. Kelly, S. M. Miller, V. Dötsch, *J. Am. Chem. Soc.* **2001**, *123*, 2446 – 2447.
[33] Z. Serber, L. Corsini, F. Durst, V. Dötsch, *Methods Enzymol.* **2005**, *394*, 17 – 41.
[34] Z. Serber, P. Selenko, R. Hänsel, S. Reckel, F. Löhr, J. E. Ferrell, V. Dötsch, *Nat. Protoc.* **2006**, *1*, 2701 – 2709.
[35] S. Reckel, R. Haensel, F. Loehr, V. Doetsch, *Prog. Nucl. Magn. Reson. Spectrosc.* **2007**, *51*, 91 – 101.
[36] P. Selenko, G. Wagner, *J. Struct. Biol.* **2007**, *158*, 244 – 253.
[37] D. S. Burz, K. Dutta, D. Cowburn, A. Shekhtman, *Nat. Methods* **2006**, *3*, 91 – 93.
[38] D. Sakakibara, A. Sasaki, T. Ikeya, J. Hamatsu, T. Hanashima, M. Mishima, M. Yoshimasu, N. Hayashi, T. Mikawa, M. Wälchli, B. O. Smith, M. Shirakawa, P. Güntert, Y. Ito, *Nature* **2009**, *458*, 102 – 105.
[39] K. Inomata, A. Ohno, H. Tochio, S. Isogai, T. Tenno, I. Nakase, T. Takeuchi, A. Futaki, Y. Ito, H. Hiroaki, M. Shirakawa, *Nature* **2009**, *458*, 106 – 109.
[40] C. Li, Y. Wang, G. J. Pielak, *J. Phys. Chem. B* **2009**, *113*, 13390 – 13392.
[41] Y. Wang, C. Li, G. J. Pielak, *J. Am. Chem. Soc.* **2010**, *132*, 9392 – 9397.
[42] F. L. Giesel, H. von Tengg-Kobligk, I. D. Wilkinson, P. Siegler, W. Claus, M. Frank, K. Lodemann, M. Essig, *Invest. Radiol.* **2006**, *41*, 222 – 228.
[43] S. Pickup, A. K. Wood, H. L. Kundel, *Magn. Reson. Med.* **2005**, *53*, 35 – 40.
[44] G. J. Stanisz, R. M. Henkelman, *Magn. Reson. Med.* **2000**, *44*, 665 – 667.
[45] Y. Wang, M. Spiller, P. Caravan, *Magn. Reson. Med.* **2010**, *63*, 609 – 616.
[46] H. Johansson, M. R. Jensen, H. Gesmar, S. Meier, J. M. Vinther, C. Keeler, M. E. Hodsdon, J. J. Led, *J. Am. Chem. Soc.* **2014**, *136*, 10277 – 10286.
[47] S. Aime, M. Botta, M. Fasano, S. G. Crich, E. Terreno, *J. Biol. Inorg. Chem.* **1996**, *1*, 312 – 319.
[48] S. Laurent, L. V. Elst, R. N. Muller, *Contrast Media Mol. Imag.* **2006**, *1*, 128 – 137.
[49] A. Fontes, S. Karimi, L. Helm, P. M. Ferreira, J. P. André, *Euro. J. Inorg. Chem.* **2015**, 4798 – 4809.
[50] P. Sebastiao, D. Sousa, A. C. Ribeiro, M. Vilfan, G. Lahajnar, J. Seliger, S. Žumer, *Phys. Rev. E* **2005**, *72*, 061702.
[51] L. A. Neves, P. J. Sebastiao, I. M. Coelhoso, J. G. Crespo, *J. Phys. Chem. B* **2011**, *115*, 8713 – 8723.
[52] S. Ding, Z. Wu, K. C. Yu, P. H. Lai, *Mol. Phys.* **2009**, *107*, 2261 – 2273.
[53] R. Kimmich, E. Anoardo, *Prog. Nucl. Magn. Reson. Spectrosc.* **2004**, *44*, 257 – 320.
[54] D. Kruk, A. Herrmann, E. Rössler, *Prog. Nucl. Magn. Reson. Spectrosc.* **2012**, *63*, 33 – 64.
[55] J. P. Korb, R. G. Bryant, *J. Chem. Phys.* **2001**, *115*, 10964 – 10975.
[56] J. P. Korb, R. G. Bryant, *Magn. Reson. Med.* **2002**, *48*, 21 – 26.

[57] J. P. Korb, G. Diakova, R. G. Bryant, *J. Chem. Phys.* **2006**, *124*, 134910 – 134916.
[58] A. Roch, R. N. Muller, P. Gillis, *J. Chem. Phys.* **1999**, *110*, 5403 – 5411.
[59] V. S. Vexler, O. Clément, H. Schmitt-Willich, R. C. Brasch, *J. Magn. Reson. Imaging.* **1994**, *4*, 381 – 388.
[60] T. S. Desser, D. L. Rubin, H. H. Muller, F. Qing, S. Khodor, G. Zanazzi, S. W. Young, D. L. Ladd, J. A. Wellons, K. E. Kellar, J. L. Toner, R. A. Snow, *J. Magn. Reson. Imaging.* **1994**, *4*, 467 – 472.
[61] K. A. Majorek, P. J. Porebski, A. Dayal, M. D. Zimmerman, K. Jablonska, A. J. Stewart, M. Chruszcz, W. Minor, *Mol. Immunol.* **2012**, *52*, 174 – 182.

Received: November 29, 2017
Version of record online March 13, 2018

